Supporting Information: Energy Band Alignment Between Anatase and Rutile TiO_2

Verena Pfeifer,[†] Paul Erhart,[‡] Shunyi Li,[†] Karsten Rachut,[†] Jan Morasch,[†] Joachim Brötz,[†] Philip Reckers,[†] Thomas Mayer,[†] Sven Rühle,[¶] Arie Zaban,[¶] Iván Mora Seró,[§] Juan Bisquert,[§] Wolfram Jaegermann,[†] and Andreas Klein[*,†]

Technische Universität Darmstadt, Institute of Materials Science, D-64287 Darmstadt, Germany, Chalmers University of Technology, Department of Applied Physics, S-41296 Gothenburg, Sweden, Bar Ilan University, Department of Chemistry, 52900 Ramat Gan, Israel, and University Jaume I, Departament de Física, 12071 Castelló de la Plana, Spain

E-mail: aklein@surface.tu-darmstadt.de

[*]To whom correspondence should be addressed
[†]Technische Universität Darmstadt
[‡]Chalmers University of Technology
[¶]Bar Ilan University
[§]Universitat Jaume I

Experimental procedure and results

Sample preparation

Polycrystalline anatase thin films on quartz glass as well as rutile bulk single crystals served as substrates for the interface experiments. The 200 nm thick anatase films were deposited by reactive DC magnetron sputtering of a 99.995 % pure titanium target with a diameter of 5.08 cm. The used deposition parameters are listed in Table S1. By a subsequent 1 h heat treatment at 600 °C in 0.5 Pa O_2, the amorphous TiO_2 film transformed into the anatase structure as confirmed by grazing incidence X-ray diffraction (GIXRD) measurements (see below).

Table S1: Employed sputter deposition parameters: p describes pressure, d_{ts} target-substrate distance, Q_{Ar} Ar gas flux, Q_{O_2} O_2 gas flux, T_s substrate temperature, and P applied power.

Parameter	TiO_2	RuO_2	ITO
p / Pa	0.5	1	0.5
d_{ts} / cm	6	9.4	8.4
Q_{Ar} / sccm	19.6	9.25	6.6
Q_{O_2} / sccm	0.4	0.75	0
T_s / °C	25	25	400
P / W	30	10	25

The rutile single crystals with (001) surface orientation were purchased from CrysTec (Berlin, Germany). To prevent charging of the poorly conducting anatase and rutile substrates during the XPS measurements, they were covered with a sputtered, 100 nm thick platinum film with a central hole of 1 mm diameter leaving free a measuring spot of the substrates. The procedure has already been applied successfully to measure band alignment of other highly insulating substrates.[1] In order to obtain a clean adsorbate free substrate surface as a starting point for the deposition of either RuO_2 or ITO, the samples were heated in the deposition chamber at $500\,°C$ in $0.5\,Pa$ oxygen for $3.5\,h$. After this procedure, no carbon emissions are detected as evident in the survey spectra shown below.

RuO_2 was deposited by reactive DC magnetron sputtering of a 99.95 % pure, 5.08 cm in diameter Ru target. More details of the RuO_2 deposition and resulting film properties have been

reported elsewhere.[2] ITO films were prepared by RF magnetron sputtering of a 5.08 cm, 99.99 % pure In_2O_3:Sn target with 10 wt.% Sn content. More details of the ITO deposition and resulting film properties have been reported elsewhere.[3]

Structural analysis

The structure of the prepared TiO_2 films deposited on quartz glass was analyzed by grazing incidence X-ray diffraction (GIXRD) measurements with Cu K_α radiation using a SEIFERT XRD 30003 PTS-3 diffractometer. Figure S1 shows the diffraction pattern of a TiO_2 film deposited at room temperature and annealed at 600 °C. The indicated reflections can be attributed to the anatase crystal structure of TiO_2. As no reflections of the rutile structure are observed, it can be assumed that the annealed films are completely crystallized in the anatase structure. Therefore, the processed TiO_2 films on quartz glass were used as anatase substrates for the interface experiments.

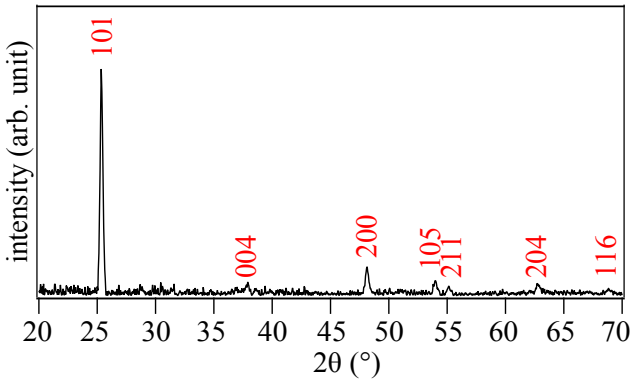

Figure S1: Diffractogram of a TiO_2 film deposited on quartz glass. All indicated reflections belong to the anatase structure (PDF card 00-021-1272).

Binding energy differences between core levels and valence band maximum

Throughout the investigation of anatase and rutile via X-ray photoelectron spectroscopy (XPS), it was observed that the binding energy differences between core level emission lines and the valence band maximum are larger in rutile than in anatase. In Fig. S2 a compilation of binding energy differences of $\Delta E_{\mathrm{O1s,VB}}$ and $\Delta E_{\mathrm{Ti2}p\mathrm{,VB}}$ is shown. The investigated samples were produced

in different manners as assigned in the graph. The binding energy differences of the rutile samples are consistently 0.45 ± 0.1 eV larger than those of the anatase samples.

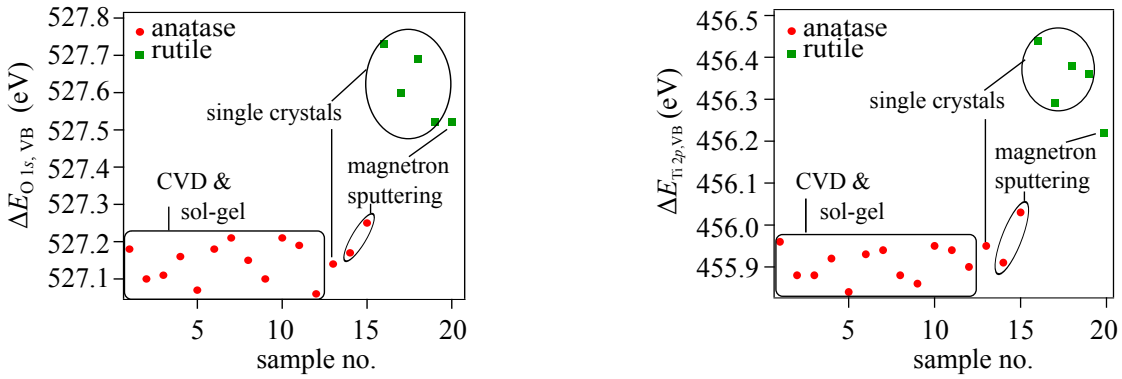

Figure S2: Binding energy differences between the O 1s (left)/Ti 2p (right) core levels and the valence band maximum of different anatase and rutile samples.

Interface experiments

The survey as well as the core level XP spectra of all four interface experiments of anatase and rutile with RuO_2 as well as with ITO are shown in this section. Throughout the interface experiments the samples remained free of any contamination as only the emission lines of the substrate and the contact material are observed in the survey spectra. The C 1s emission line, which occurs in some of the survey spectra of the substrates, can be attributed to hydrocarbon adsorbates initially covering the substrate surfaces. These contaminations were removed by the heat treatment in oxygen atmosphere described above. The evolution of the core level binding energies is extracted from the detail spectra. By subtracting the constant binding energy differences ($\Delta E_{\mathrm{CL,VB}}$), the evolution of the valence band maximum with respect to the Fermi energy ($E_{\mathrm{F}} - E_{\mathrm{VB}}$) is determined. The Fermi level serves as the binding energy reference, which is calibrated using a sputter cleaned Ag foil.

RuO_2 on anatase and rutile

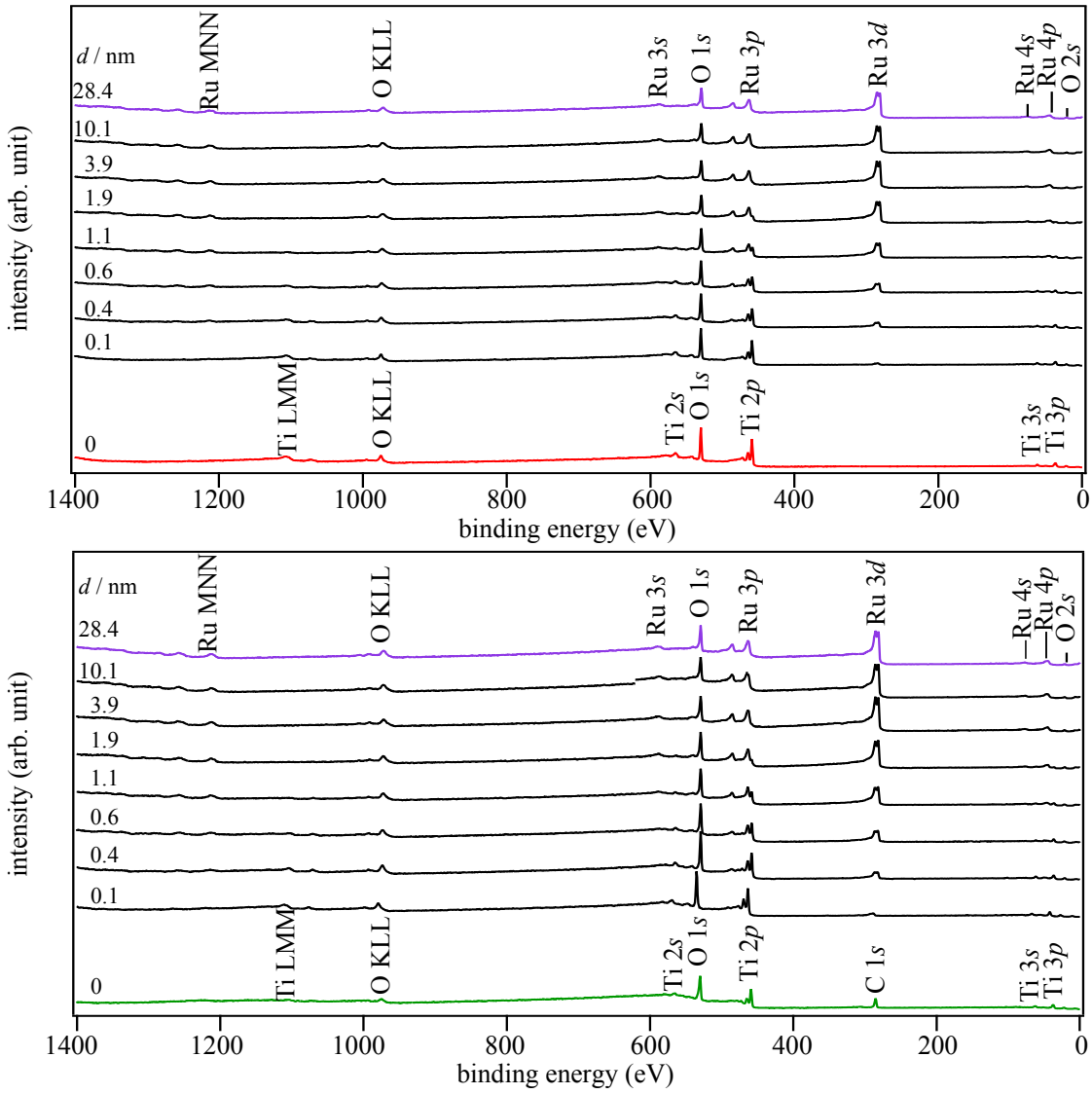

Figure S3: Survey XP spectra recorded during interface formation between anatase (top) and rutile (bottom) with RuO_2.

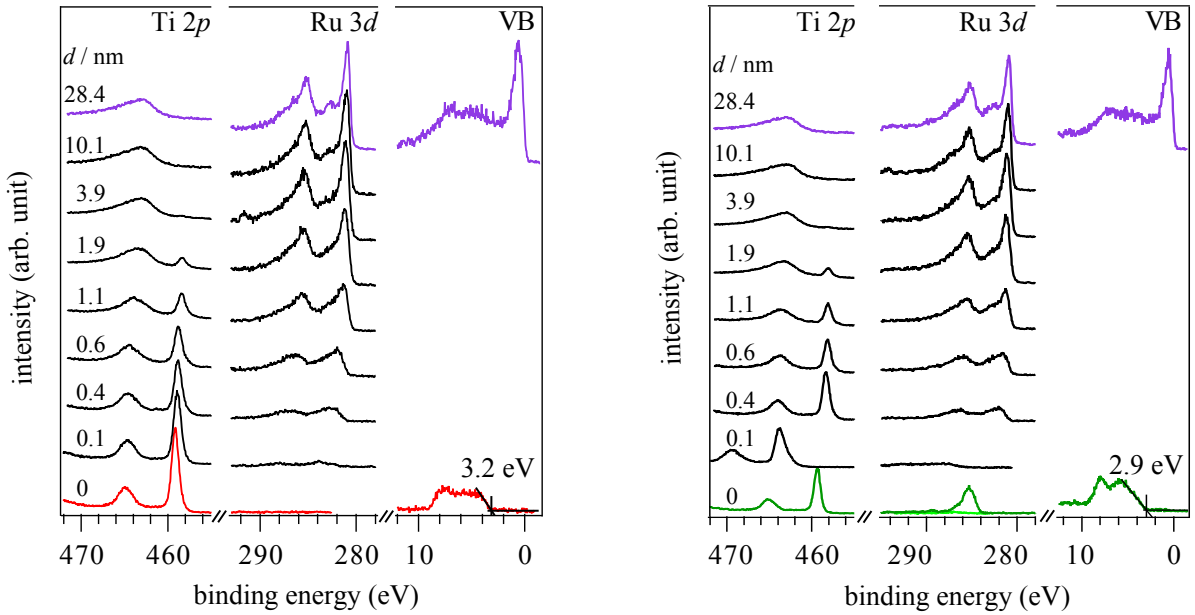

Figure S4: XP spectra of the Ti 2p and Ru 3d core levels as well as the valence band spectra of anatase (left) and rutile (right) in the course of RuO_2 deposition. The initial valence band maximum binding energies $E_F - E_{VB}$ of the anatase and rutile substrates are 3.2 ± 0.1 eV and $2.9\ pm 0.1$ eV, respectively. The non-vanishing intensity in the Ru 3d spectrum of the rutile substrate originates from the C 1s core level, which has a similar binding energy. These adsorbates are removed before RuO_2 deposition by annealing in O_2 as indicated by the light green spectra. As the sample showed charging effects after the cleaning, this spectrum had to be recorded with a charge neutralizer. Charging still occurred after the first RuO_2 deposition step but no more for higher coverage. Therefore, the recorded spectra at 0.1 nm RuO_2 thickness are shifted towards higher binding energy.

ITO on anatase and rutile

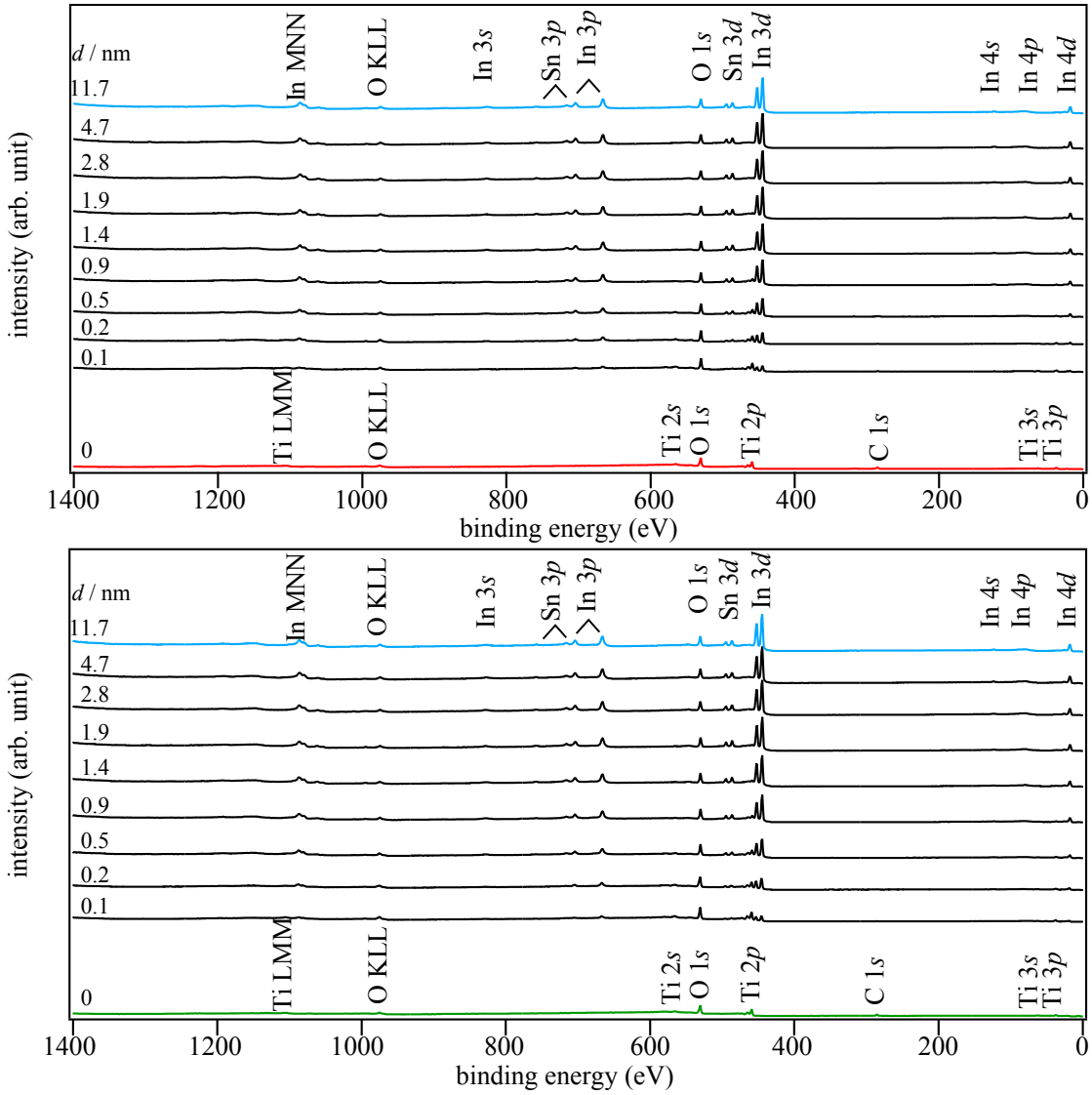

Figure S5: Survey XP spectra recorded during the interface formation between anatase (top) and rutile (bottom) with ITO.

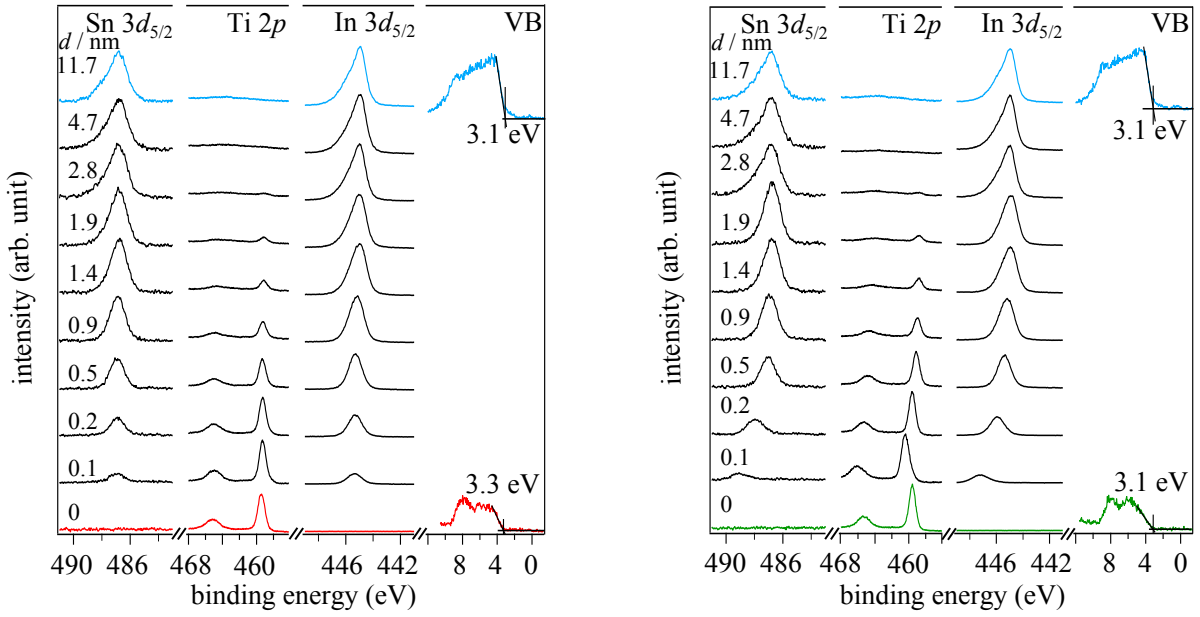

Figure S6: XP spectra of the Sn $3d_{5/2}$, Ti 2p and In $3d_{5/2}$ core levels and of the valence bands of anatase (left) and rutile (right) in the course of ITO deposition. The initial valence band maximum binding energies $E_F - E_{VB}$ of the anatase and rutile substrates are 3.3 ± 0.1 eV and 3.1 ± 0.1 eV, respectively.

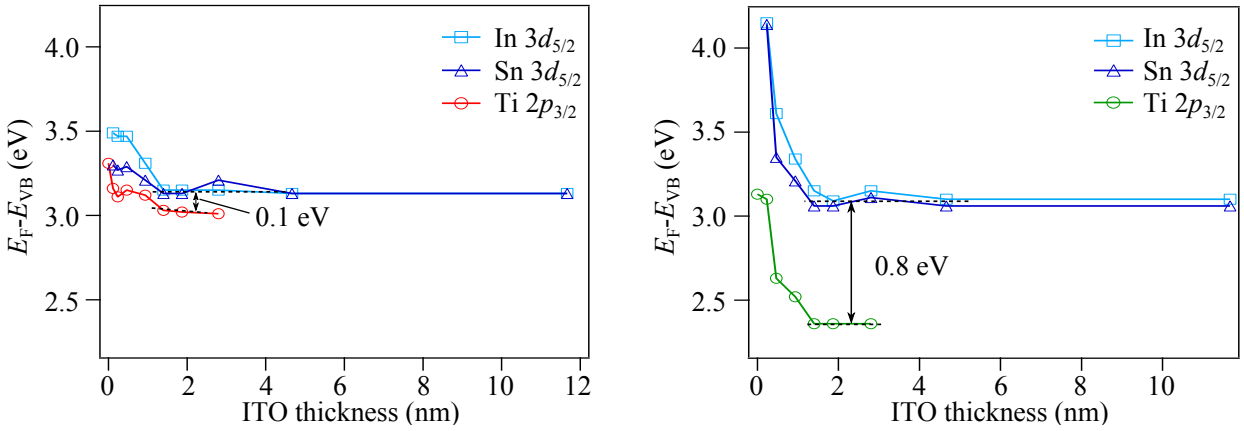

Figure S7: Evolution of the core level binding energies with increasing ITO film thickness on anatase (left) and rutile (right). For comparison, the constant $\Delta E_{CL,VB}$ are subtracted whereby the relative position of the Fermi level and the valence band maximum is obtained.

Further support for transitivity of band alignments of TiO_2

Transitivity of band alignment is fulfilled in the system RuO_2/(Ba)$SrTiO_3$ (hole Schottky barrier of $\Phi_{B,p} = 2.35 \pm 0.1$ eV[2]), $SrTiO_3$/anatase-TiO_2 ($\Delta E_{VB} = +0.04 \pm 0.1$ eV[4]) and anatase-TiO_2/RuO_2 ($\Phi_{B,p} = 2.35 \pm 0.1$ eV, see Fig. 2).

Transitivity of band alignment is also fulfilled in the system ITO/(Ba)$SrTiO_3$ ($\Delta E_{VB} = 0.05 \pm 0.1$ eV[5]), $SrTiO_3$/anatase-TiO_2 ($\Delta E_{VB} = +0.04 \pm 0.1$ eV[4]) and anatase-TiO_2/ITO ($\Delta E_{VB} = -0.1 \pm 0.1$ eV, see left part of Fig. S7).

Transitivity of band alignment is further fulfilled by the valence band offsets determined for anatase/Cu_2S ($\Delta E_{VB} = 2.9$ eV[6]), Cu_2S/CdS ($\Delta E_{VB} = -1.2$ eV[7]), CdS/In_2O_3 ($\Delta E_{VB} = -1.5$ eV[8]), and In_2O_3/anatase ($\Delta E_{VB} = -0.1$ eV, see left part of Fig. S9).

First-principles calculations

Computational methodology

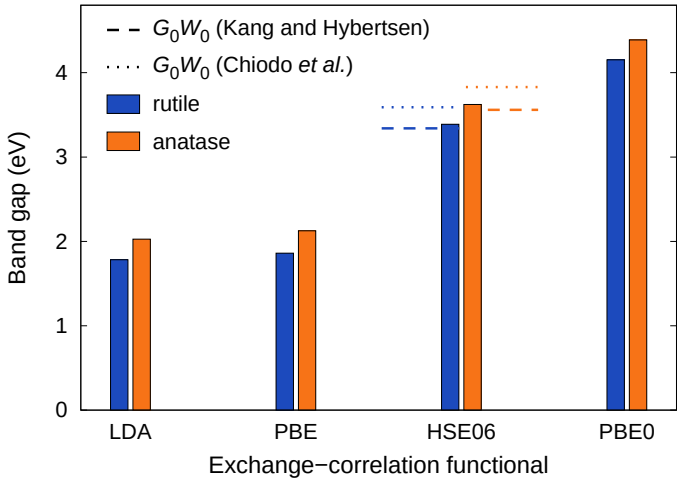

Figure S8: Band gaps for rutile and anatase obtained using different exchange-correlation functionals in comparison with G_0W_0 values.[9,10]

Calculations were carried out within density functional theory (DFT) using the projector augmented wave method[11,12] as implemented in the Vienna ab-initio simulation package.[13–16] Elec-

tronic states down to the Ti-$3p$ and O-$2s$ shells were treated as part of the valence. All calculations were carried out at the experimentally determined lattice parameters[17] and employed a plane-wave cutoff energy of 400 eV as well as a Γ-centered $6 \times 6 \times 6$ k-point mesh. The effect of the treatment of exchange and correlation (XC) on the results was tested by considering the local density approximation (LDA), the generalized gradient approximation parameterized by Perdew, Burke, and Ernzerhof (PBE),[18] an unscreened hybrid XC functional (PBE0)[19] as well as a range-separated hybrid XC functional (HSE06).[20] In the case of the hybrid XC functionals the k-point sampling was reduced by a factor of one half in the exchange part.[21] The HSE06 functional in particular has been previously found to yield band gaps and widths[22] in very good agreement with experiment[23,24] and G_0W_0 calculations.[9,10] The band gaps obtained at different levels of approximation are shown in Fig. S8. This demonstrates the very good agreement of the band gaps obtained using the HSE06 functionals and the values calculated using the G_0W_0 approach,[9,10] which in turn are in good agreement with experiment (see Refs.[9] and[10] for a more detailed comparison).

On the basis of the DFT calculations maximally localized Wannier functions (MLWFs)[25] were constructed[26,27] and subsequently employed to interpolate band structures and DOS on very dense k-point meshes with up to $41 \times 41 \times 41$ divisions. The MLWFs were also employed to interpret the nature of chemical bonding in rutile and anatase.

Band alignment

The determination of valence and conduction offsets between rutile and anatase requires alignment of the energy scales from two different sets of calculations. Previous studies employed for example branching point energies[22] and a Mott-Littleton approach.[28] In the present work we employ a more direct approach based on the alignment with respect to deep core levels as well as the electrostatic potentials at the ionic sites. A careful comparison of data from LDA calculations shows that alignment with respect to Ti-$1s$ states, Ti-$2s$ states or the electrostatic potential in the core yields practically identical results. The shifts obtained using either O-$1s$ states or the potential at the O cores differ by 0.08 eV. Compared to titanium the oxygen core is less screened from the valence

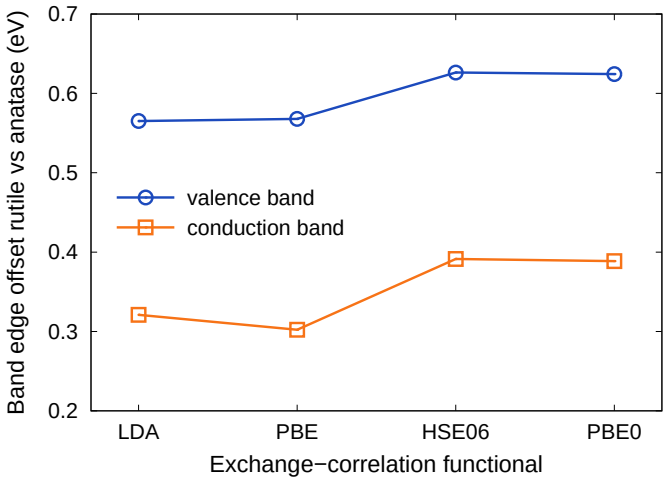

Figure S9: Band edge offsets between rutile and anatase obtained by aligning Ti core potentials.

states and accordingly more strongly affected by the crystal environment. As a result it is less well suited for band alignment. Based on this assessment we have decided to employ the electrostatic potential at the Ti cores for alignment as it permits us to analyze all four XC functionals in the same way. The valence and conduction band edge offsets obtained in this fashion are shown in Fig. S9. All functional yield qualitatively the same result. The hybrid functionals yield systematically larger offsets and values in very good agreement with experiment. Also note that HSE06 and PBE0 predict almost identical band egde offsets even though the respective band gaps differ by more than 0.5 eV.

Band structures and partial densities of states

The band structures and density of states obtained from the HSE06 functional are shown in Fig. S10. The figure illustrates the alignment of the energy scales between rutile and anatase, the similarities of the DOS and the connection between the tail in the DOS of rutile and the lone pair orbital at the valence band maximum near the Γ-point (also see Fig. 3 in the manuscript). It also serves to highlight the similar valence band widths of rutile and anatase when only the regions near the Brillouin zone boundaries (*i.e.* excluding the vicinity of the Γ-point) are considered.

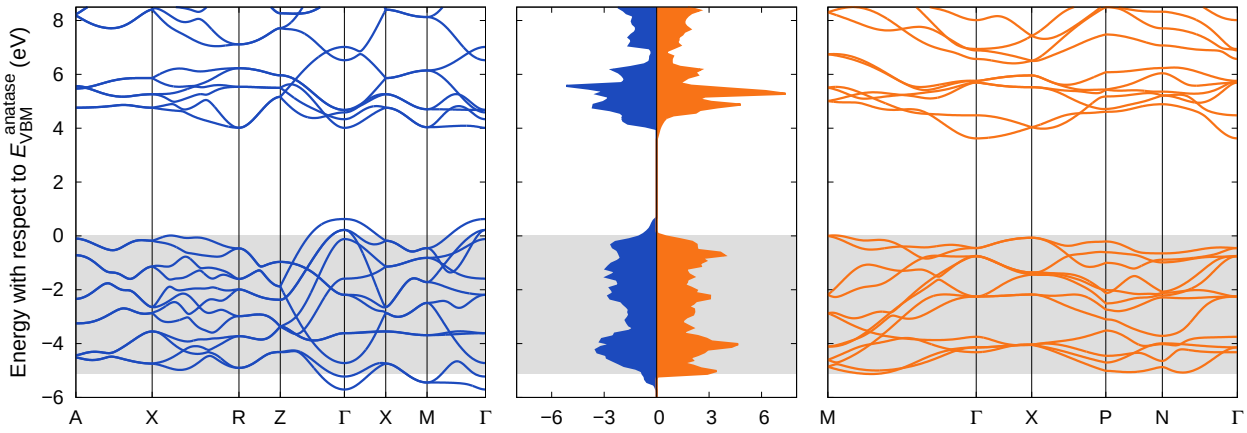

Figure S10: Band structures and densities of states of rutile (left) and anatase (right) calculated using the HSE06 exchange-correlation functional. The gray bar delineates the valence band range of anatase and serves to illustrate out the band line up between rutile and anatase.

Wannier function analysis

Maximally localized Wannier functions for rutile and anatase are shown in Figs. S11 and S12 along with the orbital projected band structures. The subpanels (f) in these figures illustrate the relative orientation and spatial distribution of the p_z-like orbitals that most strongly contribute to the topmost valence band states.

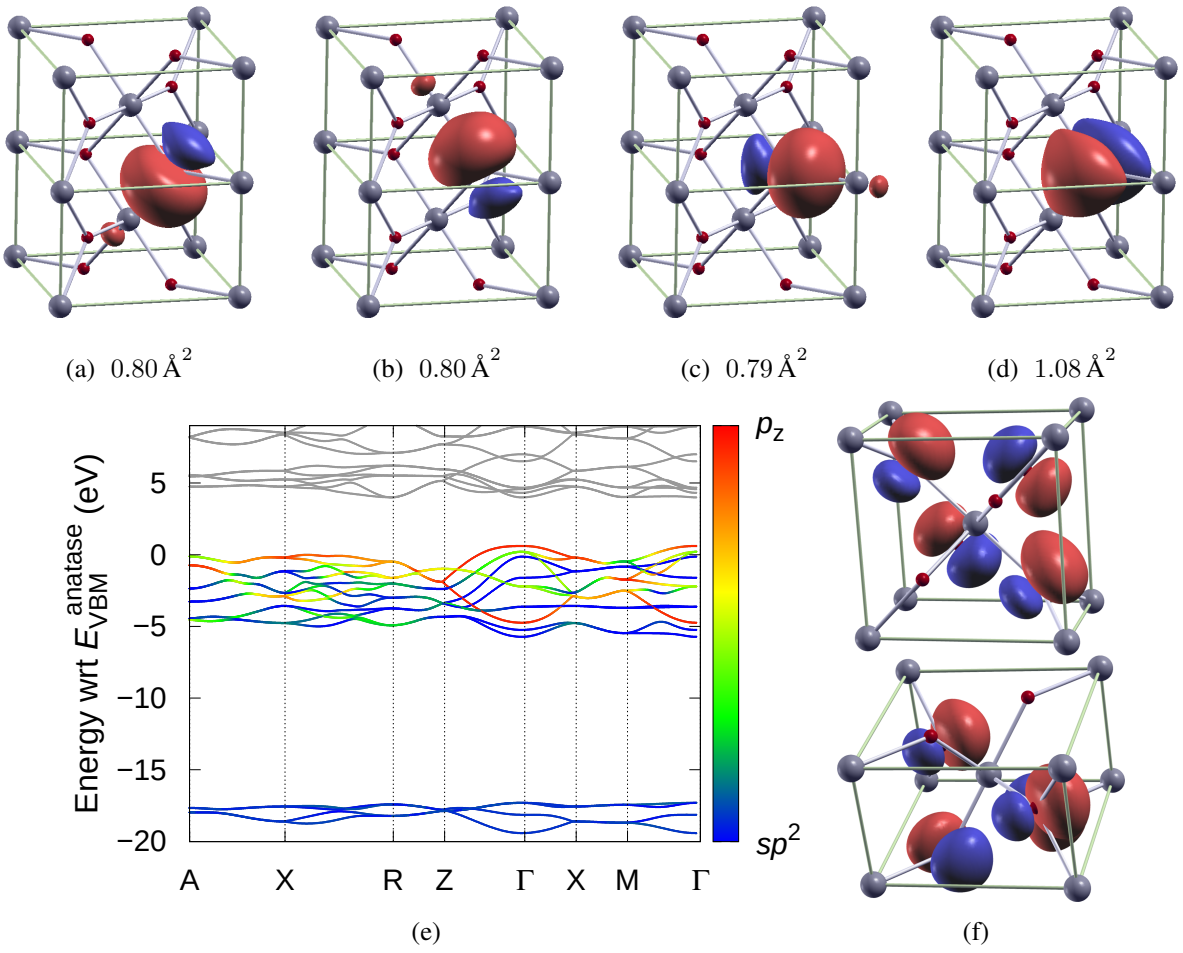

Figure S11: Representative (a-c) sp^2-like and (d) p_z-like maximally localized Wannier functions for rutile. Two primitive unit cells are shown to illustrate the bonding geometry. Orbital spreads are given in the subfigure captions. (e) Band structure of rutile. The color coding indicates the contribution of p_z-like Wannier orbitals of the type shown in (d) and (f) to the respective state. (f) Ensemble of p_z-like Wannier orbitals.

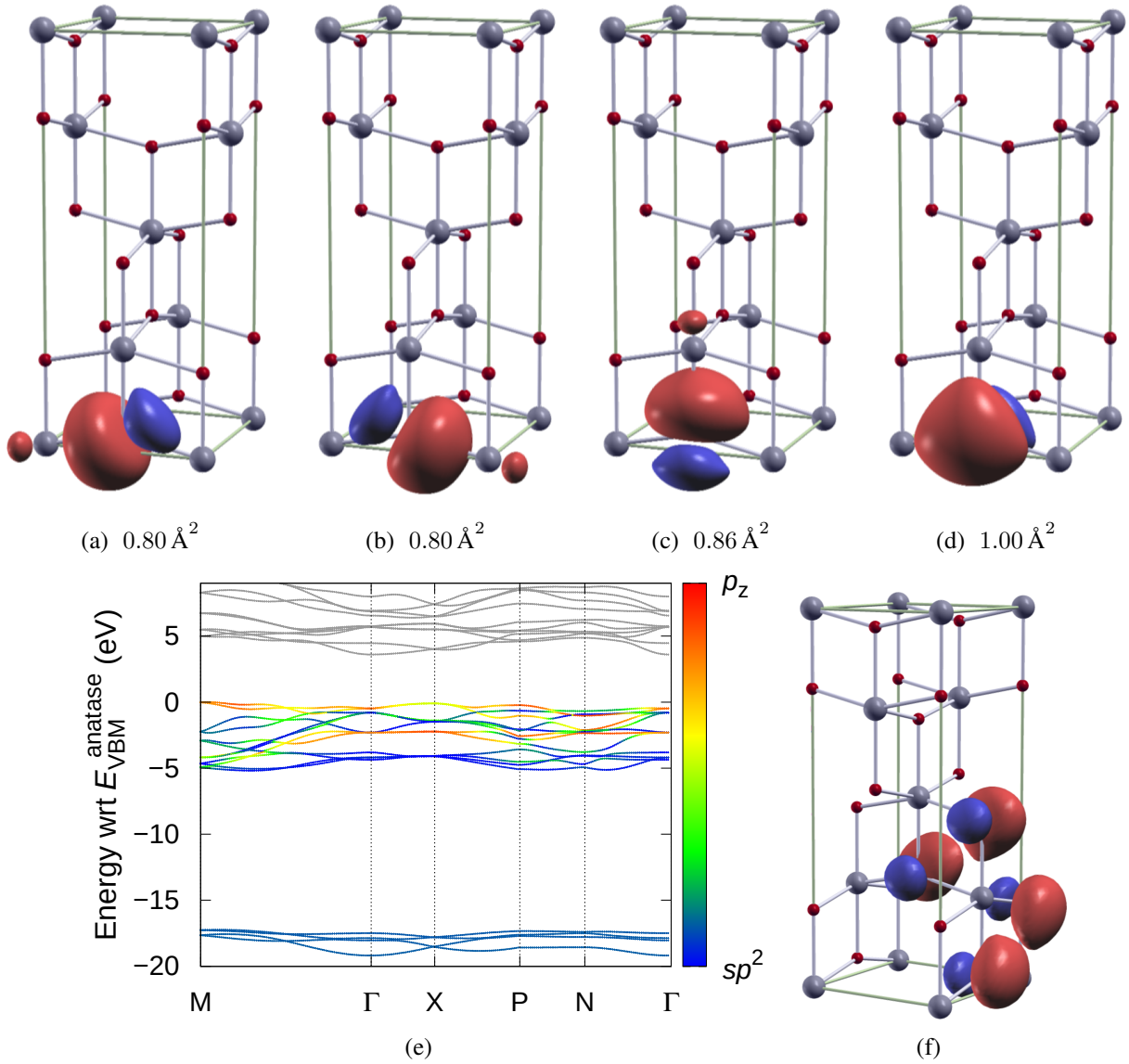

Figure S12: Representative (a-c) sp^2-like and (d) p_z-like maximally localized Wannier functions for anatase shown with respect to the conventional unit cell. Orbital spreads are given in the subfigure captions. (e) Band structure of anatase. The color coding indicates the contribution of p_z-like Wannier orbitals of the type shown in (d) and (f) to the respective state. (f) Ensemble of p_z-like Wannier orbitals.

References

(1) Chen, F.; Schafranek, R.; Wachau, A.; Zhukov, S.; Glaum, J.; Granzow, T.; von Seggern, H.; Klein, A. Barrier Heights, Polarization Switching and Electrical Fatigue in Pb(Zr,Ti)O_3 Ceramics with Different Electrodes. *J. Appl. Phys.* **2010**, *108*, 104106/1–7.

(2) Schafranek, R.; Schaffner, J.; Klein, A. In-situ Photoelectron Study of the (Ba,Sr)TiO_3/RuO_2 Contact Formation. *J. Eur. Ceram. Soc.* **2010**, *30*, 187–192.

(3) Gassenbauer, Y.; Schafranek, R.; Klein, A.; Zafeiratos, S.; Hävecker, M.; Knop-Gericke, A.; Schlögl, R. Surface States, Surface Potentials and Segregation at Surfaces of Tin-Doped In_2O_3. *Phys. Rev. B* **2006**, *73*, 245312/1–11.

(4) Chambers, S.; Ohsawa, T.; Wang, C.; Lyubinetsky, I.; Jaffe, J. Band Offsets at the Epitaxial Anatase TiO_2/*n*-$SrTiO_3$(001) Interface. *Surf. Sci.* **2009**, *603*, 771–780.

(5) Li, S.; Ghinea, C.; Bayer, T. J. M.; Motzko, M.; Schafranek, R.; Klein, A. Electrical Properties of (Ba, Sr)TiO_3 Thin Films with Pt and ITO Electrodes: Dielectric and Rectifying Behaviour. *J. Phys.: Cond. Matt.* **2011**, *23*, 334202/1–10.

(6) Liu, G.; Schulmeyer, T.; Thissen, A.; Klein, A.; Jaegermann, W. In situ Preparation and Interface Characterization of TiO_2/Cu_2S Heterointerface. *Appl. Phys. Lett.* **2003**, *82*, 2269–2271.

(7) Liu, G.; Schulmeyer, T.; Brötz, J.; Klein, A.; Jaegermann, W. Interface Properties and Band Alignment of Cu_2S/CdS Thin Film Solar Cells. *Thin Solid Films* **2003**, *431/432*, 477–482.

(8) Klein, A.; Körber, C.; Wachau, A.; Säuberlich, F.; Gassenbauer, Y.; Harvey, S. P.; Proffit, D. E.; Mason, T. O. Transparent Conducting Oxides for Photovoltaics: Manipulation of Fermi Level, Work Function and Energy Band Alignment. *Materials* **2010**, *3*, 4892–4914.

(9) Kang, W.; Hybertsen, M. S. Quasiparticle and Optical Properties of Rutile and Anatase TiO_2. *Phys. Rev. B* **2010**, *82*, 085203/1–11.

(10) Chiodo, L.; Garca-Lastra, J. M.; Iacomino, A.; Ossicini, S.; Zhao, J.; Petek, H.; Rubio, A. Self-Energy and Excitonic Effects in the Electronic and Optical Properties of TiO_2 Crystalline Phases. *Phys. Rev. B* **2010**, *82*, 045207/1–12.

(11) Blöchl, P. E. Projector Augmented-Wave Method. *Phys. Rev. B* **1994**, *50*, 17953–17979.

(12) Kresse, G.; Joubert, D. From Ultrasoft Pseudopotentials to the Projector Augmented-Wave Method. *Phys. Rev. B* **1999**, *59*, 1758–1775.

(13) Kresse, G.; Hafner, J. Ab Initio Molecular Dynamics for Liquid Metals. *Phys. Rev. B* **1993**, *47*, 558–561.

(14) Kresse, G.; Hafner, J. Ab Initio Molecular-Dynamics Simulation of the Liquid-MetalAmorphous-Semiconductor Transition in Germanium. *Phys. Rev. B* **1994**, *49*, 14251–14269.

(15) Kresse, G.; Furthmüller, J. Efficient Iterative Schemes for Ab Initio Total-Energy Calculations Using a Plane-Wave Basis Set. *Phys. Rev. B* **1996**, *54*, 11169–11186.

(16) Kresse, G.; Furthmüller, J. Efficiency of Ab-Initio Total Energy Calculations for Metals and Semiconductors Using a Plane-Wave Basis Set. *Comput. Mater. Sci.* **1996**, *6*, 15–50.

(17) Howard, C. J.; Sabine, T. M.; Dickson, F. Structural and Thermal Parameters for Rutile and Anatase. *Acta Crystallographica B* **1991**, *47*, 462–468.

(18) (a) Perdew, J.; Burke, K.; Ernzerhof, M. Generalized Gradient Approximation Made Simple. *Phys. Rev. Lett.* **1996**, *77*, 3865–3868; (b) erratum, *ibib.* **1997**, *78*, 1396.

(19) Perdew, J.; Ernzerhof, M.; Burke, K. Rationale for Mixing Exact Exchange with Density Functional Approximations. *J. Chem. Phys.* **1996**, *105*, 9982–9985.

(20) (a) Heyd, J.; Scuseria, G.; Ernzerhof, M. Hybrid Functionals Based on a Screened Coulomb Potential. *J. Chem. Phys.* **2003**, *118*, 8207–8215; (b) erratum, *ibid.* **2006**, *124*, 219906/1–1.

(21) Paier, J.; Marsman, M.; Hummer, K.; Kresse, G.; Gerber, I.; Ángyán, J. Screened Hybrid Density Functionals Applied to Solids. *J. Chem. Phys.* **2006**, *124*, 154709/1–13.

(22) Deák, P.; Aradi, B.; Frauenheim, T. Band Lineup and Charge Carrier Separation in Mixed Rutile-Anatase Systems. *J. Phys. Chem. C* **2011**, *115*, 3443–3446.

(23) Pascual, J.; Camassel, J.; Mathieu, H. Fine Structure in the Intrinsic Absorption Edge of TiO_2. *Phys. Rev. B* **1978**, *18*, 5606–5614.

(24) Tang, H.; Berger, H.; Schmid, P.; Lévy, F.; Burri, G. Photoluminescence in TiO_2 Anatase Single Crystals. *Solid State Commun.* **1993**, *87*, 847–850.

(25) Marzari, N.; Mostofi, A. A.; Yates, J. R.; Souza, I.; Vanderbilt, D. Maximally Localized Wannier Functions: Theory and Applications. *Rev. Mod. Phys.* **2012**, *84*, 1419–1475.

(26) Mostofi, A. A.; Yates, J. R.; Lee, Y.; Souza, I.; D. M. Vanderbilt, N. Wannier90: A Tool for Obtaining Maximally-Localised Wannier Functions. *Comp. Phys. Comm.* **2008**, *178*, 685–699.

(27) Åberg, D.; Erhart, P.; Crowhurst, J.; Zaug, J. M.; Goncharov, A. F.; Sadigh, B. Pressure-Induced Phase Transition in the Electronic Structure of Palladium Nitride. *Phys. Rev. B* **2010**, *82*, 104116.

(28) Scanlon, D. O.; Dunnill, C. W.; Buckeridge, J.; Shevlin, S. A.; Logsdail, A. J.; Woodley, S. M.; Catlow, C. R. A.; Powell, M. J.; Palgrave, R. G.; Parkin, I. P. et al. Band Alignment of Rutile and Anatase TiO_2. *Nat. Mater.* **2013**, *12*, 798–801.